

Search for the Rare Decays $B \rightarrow K\ell^+\ell^-$ and $B \rightarrow K^*(892)\ell^+\ell^-$

The BABAR Collaboration

Abstract

We present preliminary results from a search for the flavor-changing neutral current decays $B \rightarrow K\ell^+\ell^-$ and $B \rightarrow K^*(892)\ell^+\ell^-$ using a sample of $22.7 \times 10^6 \Upsilon(4S) \rightarrow B\bar{B}$ decays collected with the BABAR detector at the PEP-II B Factory. We have reconstructed the following final states: $B^+ \rightarrow K^+\ell^+\ell^-$, $B^0 \rightarrow K^0\ell^+\ell^-$ ($K_s^0 \rightarrow \pi^+\pi^-$), $B^+ \rightarrow K^{*+}\ell^+\ell^-$ ($K^{*+} \rightarrow K_s^0\pi^+$), and $B^0 \rightarrow K^{*0}\ell^+\ell^-$ ($K^{*0} \rightarrow K^+\pi^-$), where $\ell^+\ell^-$ is either an e^+e^- or $\mu^+\mu^-$ pair. We obtain the 90% C.L. upper limits $\mathcal{B}(B \rightarrow K\ell^+\ell^-) < 0.6 \times 10^{-6}$ and $\mathcal{B}(B \rightarrow K^*\ell^+\ell^-) < 2.5 \times 10^{-6}$, close to the Standard Model predictions for these branching fractions.

Submitted to the International Europhysics Conference on High Energy Physics,
7/12—7/18/2001, Budapest, Hungary

Stanford Linear Accelerator Center, Stanford University, Stanford, CA 94309

Work supported in part by Department of Energy contract DE-AC03-76SF00515.

The BABAR Collaboration,

B. Aubert, D. Boutigny, J.-M. Gaillard, A. Hicheur, Y. Karyotakis, J. P. Lees, P. Robbe, V. Tisserand
Laboratoire de Physique des Particules, F-74941 Annecy-le-Vieux, France

A. Palano

Università di Bari, Dipartimento di Fisica and INFN, I-70126 Bari, Italy

G. P. Chen, J. C. Chen, N. D. Qi, G. Rong, P. Wang, Y. S. Zhu
Institute of High Energy Physics, Beijing 100039, China

G. Eigen, P. L. Reinertsen, B. Stugu

University of Bergen, Inst. of Physics, N-5007 Bergen, Norway

B. Abbott, G. S. Abrams, A. W. Borgland, A. B. Breon, D. N. Brown, J. Button-Shafer, R. N. Cahn,
A. R. Clark, M. S. Gill, A. V. Gritsan, Y. Groysman, R. G. Jacobsen, R. W. Kadel, J. Kadyk, L. T. Kerth,
S. Kluth, Yu. G. Kolomensky, J. F. Kral, C. LeClerc, M. E. Levi, T. Liu, G. Lynch, A. B. Meyer,
M. Momayezi, P. J. Oddone, A. Perazzo, M. Pripstein, N. A. Roe, A. Romosan, M. T. Ronan,
V. G. Shelkov, A. V. Telnov, W. A. Wenzel

Lawrence Berkeley National Laboratory and University of California, Berkeley, CA 94720, USA

P. G. Bright-Thomas, T. J. Harrison, C. M. Hawkes, D. J. Knowles, S. W. O'Neale, R. C. Penny,
A. T. Watson, N. K. Watson

University of Birmingham, Birmingham, B15 2TT, United Kingdom

T. Deppermann, K. Goetzen, H. Koch, J. Krug, M. Kunze, B. Lewandowski, K. Peters, H. Schmuecker,
M. Steinke

Ruhr Universität Bochum, Institut für Experimentalphysik 1, D-44780 Bochum, Germany

J. C. Andress, N. R. Barlow, W. Bhimji, N. Chevalier, P. J. Clark, W. N. Cottingham, N. De Groot,
N. Dyce, B. Foster, J. D. McFall, D. Wallom, F. F. Wilson

University of Bristol, Bristol BS8 1TL, United Kingdom

K. Abe, C. Hearty, T. S. Mattison, J. A. McKenna, D. Thiessen
University of British Columbia, Vancouver, BC, Canada V6T 1Z1

S. Jolly, A. K. McKemey, J. Tinslay

Brunel University, Uxbridge, Middlesex UB8 3PH, United Kingdom

V. E. Blinov, A. D. Bukin, D. A. Bukin, A. R. Buzykaev, V. B. Golubev, V. N. Ivanchenko, A. A. Korol,
E. A. Kravchenko, A. P. Onuchin, A. A. Salnikov, S. I. Serednyakov, Yu. I. Skovpen, V. I. Telnov,
A. N. Yushkov

Budker Institute of Nuclear Physics, Novosibirsk 630090, Russia

D. Best, A. J. Lankford, M. Mandelkern, S. McMahon, D. P. Stoker
University of California at Irvine, Irvine, CA 92697, USA

A. Ahsan, K. Arisaka, C. Buchanan, S. Chun

University of California at Los Angeles, Los Angeles, CA 90024, USA

- J. G. Branson, D. B. MacFarlane, S. Prell, Sh. Rahatlou, G. Raven, V. Sharma
University of California at San Diego, La Jolla, CA 92093, USA
- C. Campagnari, B. Dahmes, P. A. Hart, N. Kuznetsova, S. L. Levy, O. Long, A. Lu, J. D. Richman,
W. Verkerke, M. Witherell, S. Yellin
University of California at Santa Barbara, Santa Barbara, CA 93106, USA
- J. Beringer, D. E. Dorfan, A. M. Eisner, A. Frey, A. A. Grillo, M. Grothe, C. A. Heusch, R. P. Johnson,
W. Kroeger, W. S. Lockman, T. Pulliam, H. Sadrozinski, T. Schalk, R. E. Schmitz, B. A. Schumm,
A. Seiden, M. Turri, W. Walkowiak, D. C. Williams, M. G. Wilson
University of California at Santa Cruz, Institute for Particle Physics, Santa Cruz, CA 95064, USA
- E. Chen, G. P. Dubois-Felsmann, A. Dvoretzkii, D. G. Hitlin, S. Metzler, J. Oyang, F. C. Porter, A. Ryd,
A. Samuel, M. Weaver, S. Yang, R. Y. Zhu
California Institute of Technology, Pasadena, CA 91125, USA
- S. Devmal, T. L. Geld, S. Jayatilake, G. Mancinelli, B. T. Meadows, M. D. Sokoloff
University of Cincinnati, Cincinnati, OH 45221, USA
- T. Barillari, P. Bloom, M. O. Dima, S. Fahey, W. T. Ford, D. R. Johnson, U. Nauenberg, A. Olivas,
H. Park, P. Rankin, J. Roy, S. Sen, J. G. Smith, W. C. van Hoek, D. L. Wagner
University of Colorado, Boulder, CO 80309, USA
- J. Blouw, J. L. Harton, M. Krishnamurthy, A. Soffer, W. H. Toki, R. J. Wilson, J. Zhang
Colorado State University, Fort Collins, CO 80523, USA
- T. Brandt, J. Brose, T. Colberg, G. Dahlinger, M. Dickopp, R. S. Dubitzky, A. Hauke, E. Maly,
R. Müller-Pfefferkorn, S. Otto, K. R. Schubert, R. Schwierz, B. Spaan, L. Wilden
Technische Universität Dresden, Institut für Kern- und Teilchenphysik, D-01062, Dresden, Germany
- L. Behr, D. Bernard, G. R. Bonneaud, F. Brochard, J. Cohen-Tanugi, S. Ferrag, E. Roussot, S. T’Jampens,
Ch. Thiebaux, G. Vasileiadis, M. Verderi
Ecole Polytechnique, F-91128 Palaiseau, France
- A. Anjomshoaa, R. Bernet, A. Khan, D. Lavin, F. Muheim, S. Playfer, J. E. Swain
University of Edinburgh, Edinburgh EH9 3JZ, United Kingdom
- M. Falbo
Elon University, Elon University, NC 27244-2010, USA
- C. Borean, C. Bozzi, S. Dittongo, M. Folegani, L. Piemontese
Università di Ferrara, Dipartimento di Fisica and INFN, I-44100 Ferrara, Italy
- E. Treadwell
Florida A&M University, Tallahassee, FL 32307, USA
- F. Anulli,¹ R. Baldini-Ferrolì, A. Calcaterra, R. de Sangro, D. Falciari, G. Finocchiaro, P. Patteri,
I. M. Peruzzi,² M. Piccolo, Y. Xie, A. Zallo
Laboratori Nazionali di Frascati dell’INFN, I-00044 Frascati, Italy

¹ Also with Università di Perugia, I-06100 Perugia, Italy

S. Bagnasco, A. Buzzo, R. Contri, G. Crosetti, P. Fabbricatore, S. Farinon, M. Lo Vetere, M. Macri,
M. R. Monge, R. Musenich, M. Pallavicini, R. Parodi, S. Passaggio, F. C. Pastore, C. Patrignani,
M. G. Pia, C. Priano, E. Robutti, A. Santroni

Università di Genova, Dipartimento di Fisica and INFN, I-16146 Genova, Italy

M. Morii

Harvard University, Cambridge, MA 02138, USA

R. Bartoldus, T. Dignan, R. Hamilton, U. Mallik

University of Iowa, Iowa City, IA 52242, USA

J. Cochran, H. B. Crawley, P.-A. Fischer, J. Lamsa, W. T. Meyer, E. I. Rosenberg

Iowa State University, Ames, IA 50011-3160, USA

M. Benkebil, G. Grosdidier, C. Hast, A. Höcker, H. M. Lacker, S. Laplace, V. Lepeltier, A. M. Lutz,
S. Plaszczynski, M. H. Schune, S. Trincaz-Duvoid, A. Valassi, G. Wormser

Laboratoire de l'Accélérateur Linéaire, F-91898 Orsay, France

R. M. Bionta, V. Brigljević, D. J. Lange, M. Mugge, X. Shi, K. van Bibber, T. J. Wenaus, D. M. Wright,
C. R. Wuest

Lawrence Livermore National Laboratory, Livermore, CA 94550, USA

M. Carroll, J. R. Fry, E. Gabathuler, R. Gamet, M. George, M. Kay, D. J. Payne, R. J. Sloane,
C. Touramanis

University of Liverpool, Liverpool L69 3BX, United Kingdom

M. L. Aspinwall, D. A. Bowerman, P. D. Dauncey, U. Egede, I. Eschrich, N. J. W. Gunawardane,
J. A. Nash, P. Sanders, D. Smith

University of London, Imperial College, London, SW7 2BW, United Kingdom

D. E. Azzopardi, J. J. Back, P. Dixon, P. F. Harrison, R. J. L. Potter, H. W. Shorthouse, P. Strother,
P. B. Vidal, M. I. Williams

Queen Mary, University of London, E1 4NS, United Kingdom

G. Cowan, S. George, M. G. Green, A. Kurup, C. E. Marker, P. McGrath, T. R. McMahon, S. Ricciardi,
F. Salvatore, I. Scott, G. Vaitsas

University of London, Royal Holloway and Bedford New College, Egham, Surrey TW20 0EX, United Kingdom

D. Brown, C. L. Davis

University of Louisville, Louisville, KY 40292, USA

J. Allison, R. J. Barlow, J. T. Boyd, A. C. Forti, J. Fullwood, F. Jackson, G. D. Lafferty, N. Savvas,
E. T. Simopoulos, J. H. Weatherall

University of Manchester, Manchester M13 9PL, United Kingdom

A. Farbin, A. Jawahery, V. Lillard, J. Olsen, D. A. Roberts, J. R. Schieck

University of Maryland, College Park, MD 20742, USA

G. Blaylock, C. Dallapiccola, K. T. Flood, S. S. Hertzbach, R. Kofler, T. B. Moore, H. Staengle, S. Willocq

University of Massachusetts, Amherst, MA 01003, USA

B. Brau, R. Cowan, G. Sciolla, F. Taylor, R. K. Yamamoto
Massachusetts Institute of Technology, Laboratory for Nuclear Science, Cambridge, MA 02139, USA

M. Milek, P. M. Patel, J. Trischuk
McGill University, Montréal, Canada QC H3A 2T8

F. Lanni, F. Palombo
Università di Milano, Dipartimento di Fisica and INFN, I-20133 Milano, Italy

J. M. Bauer, M. Booke, L. Cremaldi, V. Eschenburg, R. Kroeger, J. Reidy, D. A. Sanders, D. J. Summers
University of Mississippi, University, MS 38677, USA

J. P. Martin, J. Y. Nief, R. Seitz, P. Taras, A. Woch, V. Zacek
Université de Montréal, Laboratoire René J. A. Lévesque, Montréal, Canada QC H3C 3J7

H. Nicholson, C. S. Sutton
Mount Holyoke College, South Hadley, MA 01075, USA

C. Cartaro, N. Cavallo,³ G. De Nardo, F. Fabozzi, C. Gatto, L. Lista, P. Paolucci, D. Piccolo, C. Sciacca
Università di Napoli Federico II, Dipartimento di Scienze Fisiche and INFN, I-80126, Napoli, Italy

J. M. LoSecco
University of Notre Dame, Notre Dame, IN 46556, USA

J. R. G. Alsmiller, T. A. Gabriel, T. Handler
Oak Ridge National Laboratory, Oak Ridge, TN 37831, USA

J. Brau, R. Frey, M. Iwasaki, N. B. Sinev, D. Strom
University of Oregon, Eugene, OR 97403, USA

F. Colecchia, F. Dal Corso, A. Dorigo, F. Galeazzi, M. Margoni, G. Michelon, M. Morandin, M. Posocco,
M. Rotondo, F. Simonetto, R. Stroili, E. Torassa, C. Voci
Università di Padova, Dipartimento di Fisica and INFN, I-35131 Padova, Italy

M. Benayoun, H. Briand, J. Chauveau, P. David, Ch. de la Vaissière, L. Del Buono, O. Hamon, F. Le
Diberder, Ph. Leruste, J. Lory, L. Roos, J. Stark, S. Versillé
Universités Paris VI et VII, Lab de Physique Nucléaire H. E., F-75252 Paris, France

P. F. Manfredi, V. Re, V. Speziali
Università di Pavia, Dipartimento di Elettronica and INFN, I-27100 Pavia, Italy

E. D. Frank, L. Gladney, Q. H. Guo, J. H. Panetta
University of Pennsylvania, Philadelphia, PA 19104, USA

C. Angelini, G. Batignani, S. Bettarini, M. Bondioli, M. Carpinelli, F. Forti, M. A. Giorgi, A. Lusiani,
F. Martinez-Vidal, M. Morganti, N. Neri, E. Paoloni, M. Rama, G. Rizzo, F. Sandrelli, G. Simi,
G. Triggiani, J. Walsh
Università di Pisa, Scuola Normale Superiore and INFN, I-56010 Pisa, Italy

³ Also with Università della Basilicata, I-85100 Potenza, Italy

M. Haire, D. Judd, K. Paick, L. Turnbull, D. E. Wagoner
Prairie View A&M University, Prairie View, TX 77446, USA

J. Albert, C. Bula, P. Elmer, C. Lu, K. T. McDonald, V. Miftakov, S. F. Schaffner, A. J. S. Smith,
A. Tumanov, E. W. Varnes
Princeton University, Princeton, NJ 08544, USA

G. Cavoto, D. del Re, R. Faccini,⁴ F. Ferrarotto, F. Ferroni, K. Fratini, E. Lamanna, E. Leonardi,
M. A. Mazzone, S. Morganti, G. Piredda, F. Safai Tehrani, M. Serra, C. Voena
Università di Roma La Sapienza, Dipartimento di Fisica and INFN, I-00185 Roma, Italy

S. Christ, R. Waldi
Universität Rostock, D-18051 Rostock, Germany

P. F. Jacques, M. Kalelkar, R. J. Plano
Rutgers University, New Brunswick, NJ 08903, USA

T. Adye, B. Franek, N. I. Geddes, G. P. Gopal, S. M. Xella
Rutherford Appleton Laboratory, Chilton, Didcot, Oxon, OX11 0QX, United Kingdom

R. Aleksan, G. De Domenico, S. Emery, A. Gaidot, S. F. Ganzhur, P.-F. Giraud, G. Hamel de
Monchenault, W. Kozanecki, M. Langer, G. W. London, B. Mayer, B. Serfass, G. Vasseur, Ch. Yèche,
M. Zito
DAPNIA, Commissariat à l'Energie Atomique/Saclay, F-91191 Gif-sur-Yvette, France

N. Coptý, M. V. Purohit, H. Singh, F. X. Yumiceva
University of South Carolina, Columbia, SC 29208, USA

I. Adam, P. L. Anthony, D. Aston, K. Baird, J. P. Berger, E. Bloom, A. M. Boyarski, F. Bulos,
G. Calderini, R. Claus, M. R. Convery, D. P. Coupal, D. H. Coward, J. Dorfan, M. Doser, W. Dunwoodie,
R. C. Field, T. Glanzman, G. L. Godfrey, S. J. Gowdy, P. Grosso, T. Himel, T. Hryn'ova, M. E. Huffer,
W. R. Innes, C. P. Jessop, M. H. Kelsey, P. Kim, M. L. Kocian, U. Langenegger, D. W. G. S. Leith,
S. Luitz, V. Luth, H. L. Lynch, H. Marsiske, S. Menke, R. Messner, K. C. Moffeit, R. Mount, D. R. Muller,
C. P. O'Grady, M. Perl, S. Petrak, H. Quinn, B. N. Ratcliff, S. H. Robertson, L. S. Rochester,
A. Roodman, T. Schietinger, R. H. Schindler, J. Schwiening, V. V. Serbo, A. Snyder, A. Soha,
S. M. Spanier, J. Stelzer, D. Su, M. K. Sullivan, H. A. Tanaka, J. Va'vra, S. R. Wagner,
A. J. R. Weinstein, W. J. Wisniewski, D. H. Wright, C. C. Young
Stanford Linear Accelerator Center, Stanford, CA 94309, USA

P. R. Burchat, C. H. Cheng, D. Kirkby, T. I. Meyer, C. Roat
Stanford University, Stanford, CA 94305-4060, USA

R. Henderson
TRIUMF, Vancouver, BC, Canada V6T 2A3

W. Bugg, H. Cohn, A. W. Weidemann
University of Tennessee, Knoxville, TN 37996, USA

⁴ Also with University of California at San Diego, La Jolla, CA 92093, USA

J. M. Izen, I. Kitayama, X. C. Lou, M. Turcotte
University of Texas at Dallas, Richardson, TX 75083, USA

F. Bianchi, M. Bona, B. Di Girolamo, D. Gamba, A. Smol, D. Zanin
Università di Torino, Dipartimento di Fisica Sperimentale and INFN, I-10125 Torino, Italy

L. Bosisio, G. Della Ricca, L. Lanceri, A. Pompili, P. Poropat, M. Prest, E. Vallazza, G. Vuagnin
Università di Trieste, Dipartimento di Fisica and INFN, I-34127 Trieste, Italy

R. S. Panvini
Vanderbilt University, Nashville, TN 37235, USA

C. M. Brown, A. De Silva, R. Kowalewski, J. M. Roney
University of Victoria, Victoria, BC, Canada V8W 3P6

H. R. Band, E. Charles, S. Dasu, F. Di Lodovico, A. M. Eichenbaum, H. Hu, J. R. Johnson, R. Liu,
J. Nielsen, Y. Pan, R. Prepost, I. J. Scott, S. J. Sekula, J. H. von Wimmersperg-Toeller, S. L. Wu, Z. Yu,
H. Zobernig
University of Wisconsin, Madison, WI 53706, USA

T. M. B. Kordich, H. Neal
Yale University, New Haven, CT 06511, USA

1 Introduction

The flavor-changing neutral current (FCNC) decays $B \rightarrow K\ell^+\ell^-$ and $B \rightarrow K^*(892)\ell^+\ell^-$, where ℓ^\pm is a charged lepton, are highly suppressed in the Standard Model, with branching fractions predicted to be of order $10^{-7} - 10^{-6}$. The dominant contributions arise at the one-loop level and involve a $b \rightarrow t \rightarrow s$ transition, so these decays are sensitive to the Cabibbo-Kobayashi-Maskawa factor $V_{ts}^*V_{tb}$. The loop can involve either the emission and reabsorption of a virtual W -boson, with the radiation of a virtual photon or Z (that subsequently materializes into the $\ell^+\ell^-$ pair), or the emission of two virtual W bosons, producing the $\ell^+\ell^-$ pair through a box diagram. Such processes are known as electroweak penguins. The simpler decays $B \rightarrow K^*\gamma$ and $B \rightarrow X_s\gamma$ (where X_s is any hadronic system with strangeness) have been observed [1, 2], providing the first evidence for the electromagnetic penguin amplitude.

These rare decays are interesting not only as a probe of Standard Model loop effects, but also because their rates and kinematic distributions are sensitive to new, heavy particles that can appear virtually in the loop [3]. Such heavy particles are predicted, for example, by supersymmetry (SUSY) models.

Table 1 lists the predictions of a number of calculations based on the Standard Model. In such calculations, the short-distance physics that governs free-quark decay is incorporated into the Wilson coefficients C_7^{eff} , C_9^{eff} , and C_{10} in the Operator Product Expansion [10] of the effective Hamiltonian. This part of the calculation is relatively well understood in the Standard Model, except for nonperturbative contributions in the dilepton mass regions near the charmonium resonances. There are, however, significant uncertainties in the predicted rates, which arise from strong (QCD) interactions among the quarks. Although these long-distance effects are difficult to calculate, they can be rigorously parametrized in terms of form factors, which are estimated with methods such as light-cone QCD sum rules or lattice QCD. From Table 1, we see that the rate for $B \rightarrow K^*\ell^+\ell^-$ is expected to be three to four times larger than that for $B \rightarrow K\ell^+\ell^-$. The amplitudes for the $B \rightarrow K^*\ell^+\ell^-$ modes include a pole at $q^2 = m_{\ell^+\ell^-}^2 = 0$, where the photon is on the mass shell. This pole gives a substantial contribution to the rate for kinematic configurations in which $q^2 \approx 0$ and is particularly large in the $B \rightarrow K^*e^+e^-$ mode. Measurements of $B \rightarrow X_s\gamma$ constrain the magnitude of C_7^{eff} , the coefficient of the electromagnetic penguin operator, but new physics could still affect the phase of C_7^{eff} .

We search for B -meson decays in the following channels: $B^+ \rightarrow K^+\ell^+\ell^-$, $B^0 \rightarrow K^0\ell^+\ell^-$ ($K_s^0 \rightarrow \pi^+\pi^-$), $B^+ \rightarrow K^{*+}\ell^+\ell^-$ ($K^{*+} \rightarrow K_s^0\pi^+$), $B^0 \rightarrow K^{*0}\ell^+\ell^-$ ($K^{*0} \rightarrow K^+\pi^-$) where $\ell^+\ell^-$ is either an e^+e^- or a $\mu^+\mu^-$ pair. Throughout this paper, charge conjugate modes are implied.

Model	$\mathcal{B}/10^{-6}$		
	$K\ell^+\ell^-$	$K^*e^+e^-$	$K^*\mu^+\mu^-$
LCSR [3]	$0.57^{+0.17}_{-0.10}$	$2.3^{+0.7}_{-0.5}$	$1.9^{+0.5}_{-0.4}$
LCSR [4, 5]			1.4
Quark Models [6, 7]	0.62 ± 0.13	2.1 ± 0.7	1.5 ± 0.6
QCD Sum Rules [8, 9]	0.3		1.0

Table 1: Branching fraction predictions in various models within the Standard Model framework: light cone QCD sum rules (LCSR), quark models, and QCD sum rules.

2 Detector Description and Data Samples

The data used in the analysis were collected with the *BABAR* detector at the PEP-II storage ring at the Stanford Linear Accelerator Center. We analyzed the data taken in the 1999–2000 run, consisting of a 20.7 fb^{-1} sample taken on the $\Upsilon(4S)$ resonance, as well as 2.6 fb^{-1} taken at a center-of-mass energy 40 MeV below the $\Upsilon(4S)$ resonance peak to obtain a pure continuum sample. Continuum events include non-resonant $e^+e^- \rightarrow q\bar{q}$ production, where $q = u, d, s, \text{ or } c$. The on-resonance sample contains $(22.7 \pm 0.4) \times 10^6 \Upsilon(4S) \rightarrow B\bar{B}$ events.

The *BABAR* detector is described in detail elsewhere [11]. All components of the detector were used for this study. Of particular importance for this analysis are the charged-particle tracking system and the detectors used for particle identification. At radii between about 3 cm and 14 cm, charged tracks are measured with high precision in a five-layer silicon vertex tracker (SVT). Tracking beyond the SVT is provided by the 40 layer drift chamber, which extends in radius from 23.6 cm to 80.9 cm. Just outside the drift chamber is the DIRC, which is a Cherenkov ring-imaging particle identification system. Cherenkov light is produced by charged tracks as they pass through an array of 144 five-meter-long fused silica quartz bars. The Cherenkov light is transmitted to the instrumented end of the bars by total internal reflection, preserving the information on the angle of the light emission with respect to the track direction. The DIRC is used for kaon identification in this analysis and is essential to our background rejection. Electrons are identified using an electromagnetic calorimeter comprising 6580 thallium-doped CsI crystals. Muons are identified in the Instrumented Flux Return (IFR), in which resistive plate chambers (RPCs) are interleaved with the iron plates of the flux return.

3 Overview of Analysis Method

Our search for $B \rightarrow K^{(*)}\ell^+\ell^-$ was guided by several key considerations. Given the predicted branching fractions and our reconstruction efficiencies (6% to 18%), we expect only a handful of observed signal events. Because the experimental signature is strong, however, it might be possible to establish a signal with a small number of events, as long as effective background suppression is achieved. But in working with small event samples, we must ensure that no bias is introduced through the event selection that could produce either an artificial enhancement of events in the signal region, or an artificial suppression of events in the sidebands used to determine the background level.

To avoid the possibility of bias, both the signal region and the sidebands used to measure the background levels are “blinded” during the process of defining the event selection criteria, so that statistical fluctuations in these regions cannot be exploited to artificially enhance a signal. Once the event selection is defined, we apply the cuts, unblind the data, and perform unbinned maximum likelihood fits to determine the signal and background yields. In these fits, the overall background level is determined from the data, with shapes derived from Monte Carlo but checked against control samples from the data. Although we define signal and sideband regions for the purpose of optimizing event selection cuts, the distinction between these regions is not relevant to the fit.

To optimize the event selection without using either the signal region or the sidebands used for the final background determination, we have used (1) full **GEANT 3** [12] Monte Carlo for signal and backgrounds, (2) high statistics fast Monte Carlo for backgrounds, and (3) a continuum data sample collected at a center-of-mass energy below the $\Upsilon(4S)$. For simulation of signal events, we have used the event generator **EvtGen** [13] to implement a full form-factor parametrization of the

decay amplitudes. The simulation provides the detailed kinematic correlations among the particles; in particular, the joint distribution in the Dalitz plot variables q^2 and lepton energy is simulated. Final-state photon radiation is simulated with the PHOTOS [14] package. The selection procedure was optimized using matrix elements from the model by Ali *et al.* [3], but the predictions from a number of other models were studied as well. About twenty thousand events were generated for each signal final state using a full GEANT 3 simulation.

To validate the Monte Carlo modeling of both the signal and backgrounds, and to determine some of the systematic errors, we have used an extensive set of control samples from the data. The modeling of distributions characterizing signal events, and the associated cut efficiencies, were checked using $B \rightarrow J/\psi K$ and $B \rightarrow J/\psi K^*$ decays (with $J/\psi \rightarrow \ell^+\ell^-$). These decays yield final states that are topologically identical to signal events (although they have a very narrow distribution in $q^2 = m_{\ell^+\ell^-}^2$). These modes are both serious backgrounds that must be suppressed and powerful control samples for understanding the signal efficiency. Another control sample is provided by reconstructed $Ke\mu$ and $K^*e\mu$ combinations, which cannot result from B decays in the Standard Model. The Monte Carlo predictions for the background shapes associated with combinatoric backgrounds can be checked using these samples. Certain individual backgrounds, especially those that peak under or near the signal, are studied with GEANT 3 Monte Carlo samples of these decays. Finally, we defined a “large sideband” region in the data that is sufficiently far from the signal that we do not need it for determining the background level, but which allows us to check that expectations for background levels based on Monte Carlo are essentially confirmed in data prior to unblinding.

The major sources of backgrounds are $\Upsilon(4S) \rightarrow B\bar{B}$ and continuum events. More specifically, these include (1) $B \rightarrow J/\psi K^{(*)}$ or $B \rightarrow \psi(2S)K^{(*)}$ events; (2) generic $B\bar{B}$ backgrounds with either two real leptons or one real lepton and one hadron misidentified as a lepton (usually a muon); (3) background from continuum processes, especially $c\bar{c}$ events with a pair of $D \rightarrow K^{(*)}\ell^+\nu$ decays, or events with hadrons faking leptons; (4) very small but potentially serious contributions from a number of B decay modes with similar topology to the signal, such as $B^+ \rightarrow D^0\pi^+$ with $D^0 \rightarrow K^-\pi^+$, in which hadrons misidentified as leptons can create a false peaking signal; and (5) $B\bar{B}$ or continuum events with photon conversions in the detector material.

A large number of Monte Carlo samples were generated to study these backgrounds. We studied $B \rightarrow J/\psi K^{(*)}$ and $B \rightarrow \psi(2S)K^{(*)}$ events using about twenty thousand GEANT 3 events in each final state. Approximately 8.4 M GEANT 3 generic $B\bar{B}$ events and about 22 M continuum events were generated. In addition, we have developed a fast, parametrized Monte Carlo and generated 220 M $B\bar{B}$ and 690 M continuum events, corresponding to 200 fb^{-1} of integrated luminosity. The realism of this simulation was enhanced by the fact that many key quantities are simulated using look-up tables with detailed information on charged-track efficiencies, particle ID efficiencies, and particle ID misidentification rates, all of which were measured in studies of data.

4 Event Selection

In the initial step of the event selection, we require that each event have at least four charged tracks and that the ratio of the second and zeroth Fox-Wolfram moments [15] be less than 0.5. This requirement provides a first suppression of continuum events, which have a more collimated (“jet-like”) event topology than $B\bar{B}$ events. We also require that the events contain two oppositely charged loosely identified leptons with laboratory-frame momenta $p > 0.5$ (1.0) GeV/ c for electron (muon) candidates. Electrons are identified primarily on the basis of E/p , where E is the energy

measured in the CsI electromagnetic calorimeter. Muons are identified mainly by the number of nuclear interaction lengths penetrated by the charged track through the detector.

The events are also required to lie within a large, rectangular region in the plane defined by two kinematic variables [11]: $m_{\text{ES}} > 5.0 \text{ GeV}/c^2$ and $|\Delta E| < 0.8 \text{ GeV}$. Because signal events contain two B mesons and no additional particles, the energy of each B in the center-of-mass (CM) frame of the $\Upsilon(4S)$ must be equal to the e^+ or e^- beam energy in the CM frame. We define

$$m_{\text{ES}} = \sqrt{(E_{\text{beam}}^*)^2 - \left(\sum_i \mathbf{p}_i^*\right)^2}$$

$$\Delta E = \sum_i \sqrt{m_i^2 + (\mathbf{p}_i^*)^2} - E_{\text{beam}}^*,$$

where E_{beam}^* is the beam energy in the CM frame, \mathbf{p}_i^* is the CM momentum of particle i in the candidate B -meson system, and m_i is the mass of particle i . For signal events, the beam-energy-substituted B mass, m_{ES} , peaks at m_B with a resolution of about 2.5 MeV. The quantity ΔE is used to determine whether a candidate system of particles has total energy consistent with the beam energy in the CM frame.

We next apply a tighter set of particle identification requirements on both leptons and hadrons. The very tight selection criteria we apply to electrons give an efficiency of about 88% assuming well measured charged tracks, with a corresponding probability for a pion to fake an electron signature of about 0.15%. For our very tight cuts, the typical muon ID efficiency for momenta greater than about 1 GeV/ c is 60%–70%, with a pion fake probability of about 2%. Electrons and positrons are required to pass a conversions veto, which suppresses e^+e^- pairs that could have come from photon conversions in the detector material. For the $B^0 \rightarrow K^{*0}\ell^+\ell^-$ channels, we reconstruct the K^{*0} in the $K^+\pi^-$ final state, while the K^{*+} in $B^+ \rightarrow K^{*+}\ell^+\ell^-$ is reconstructed in the $K_S^0\pi^+$ final state. The mass of the K^* candidate is required to be within 75 MeV/ c^2 of the mean $K^*(892)$ mass. The charged kaon daughters of the K^* are required to be identified as kaons, and all charged tracks not identified as kaons are taken to be pion candidates. The kaon identification is based on the measurement of the Cherenkov angle from the DIRC for $p > 0.6 \text{ GeV}/c$ and on the energy-loss measurements (dE/dx) from the silicon vertex tracker and the drift chamber for momenta $p < 0.6 \text{ GeV}/c$. The typical charged kaon ID efficiency is about 80% for well reconstructed tracks, with a pion fake probability of about 2%. K_S^0 candidates are reconstructed by combining two oppositely charged pions and requiring that the mass of the candidate be within 9.3 MeV/ c^2 of the mean K_S^0 mass, that the K_S^0 candidate vertex probability be greater than 0.1%, and that the distance between the vertex and the candidate B vertex be greater than 0.1 cm. For each final state we select at most one combination of particles as a B signal candidate per event. If multiple candidates occur, we select the candidate with the greatest number of drift chamber and SVT hits on the charged tracks.

Charmonium background, $B \rightarrow J/\psi K^{(*)}$ and $\psi(2S)K^{(*)}$, is suppressed by applying a veto in the ΔE vs. $m_{\ell^+\ell^-}$ plane. The boundaries of the vetos are shown in Fig. 1. It is not sufficient to remove events with dilepton masses consistent with those of the J/ψ or $\psi(2S)$, since bremsstrahlung or track mismeasurement can result in a large departure of the dilepton mass from the resonances. Charmonium events can pass this veto if one of the leptons and the kaon are misidentified as each other (“swapped”). There is also a fairly significant feed-up from the $B \rightarrow J/\psi K$ and $B \rightarrow \psi(2S)K$ modes to the $B \rightarrow K^{*}\ell^+\ell^-$ channels. Both the swapped candidates and the feed-up contributions are explicitly vetoed.

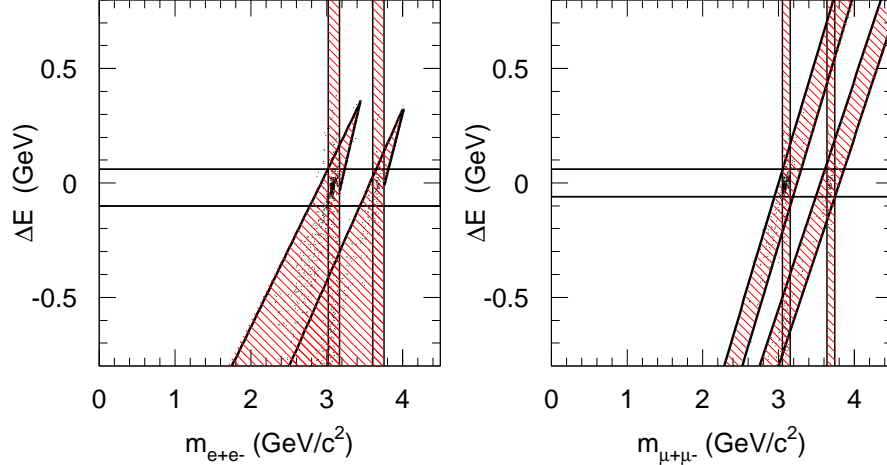


Figure 1: The veto regions in the ΔE vs. $m_{\ell+\ell-}$ plane that are populated by $B \rightarrow J/\psi K$ and $B \rightarrow \psi(2S)K$ events. The shaded areas are vetoed. (The same veto is applied to the K^* modes.) For reference, the two horizontal lines bound the region in which most signal events are found. The charmonium vetos remove these backgrounds not only from the signal region, but also from the sideband region, simplifying the description of the background in the fits.

As we have indicated, the charmonium decays $B \rightarrow J/\psi K^{(*)}$ and $B \rightarrow \psi(2S)K^{(*)}$ provide powerful control samples for checking the efficiency of our analysis cuts with events that have properties very similar to those of the signal. Figure 2 compares the ΔE distributions (absolutely normalized) of these charmonium samples in Monte Carlo vs. data. We find good agreement in both the normalization and the shape.

Continuum background is suppressed using a four-variable Fisher discriminant, which is a linear combination of the input variables with optimized coefficients. The variables are the Fox-Wolfram moment; the cosine of the angle between the B candidate and the beam axis in the CM frame ($\cos\theta_B$); the cosine of the angle between the thrust axis of the candidate B meson daughter particles and that of the rest of the event in the CM frame; and the invariant mass $m_{K\ell}$. The last variable helps discriminate against background from D semileptonic decays, for which $m_{K\ell}$ is below the D mass. $B\bar{B}$ combinatorial background is suppressed using a likelihood ratio, which combines candidate B and dilepton vertex probabilities; the significance of the dilepton separation in z (along the beam direction); $\cos\theta_B$; and the missing energy, E_{miss} , of the event in the CM frame. The variable E_{miss} provides the strongest discrimination against $B\bar{B}$ background: events with two semileptonic B decays often have more unobserved energy (due to neutrinos) than signal events.

For the purpose of optimizing the event selection, a signal box is defined in the ΔE vs. m_{ES} plane: $5.272 < m_{ES} < 5.286 \text{ GeV}/c^2$ and -0.11 (-0.07) $< \Delta E < 0.05 \text{ GeV}$ for the electron (muon) channels. Using normalizations from the GEANT 3 based Monte Carlo and shapes from the fast Monte Carlo, we perform extrapolations to estimate the number of expected signal events, S , and background events, B , in the signal region for a given set of event selection criteria. We select the criteria that minimize the probability that the backgrounds will fluctuate to a level at least as large as the predicted signal. The result of this optimization is very similar to an optimization based on maximizing $S^2/(S+B)$.

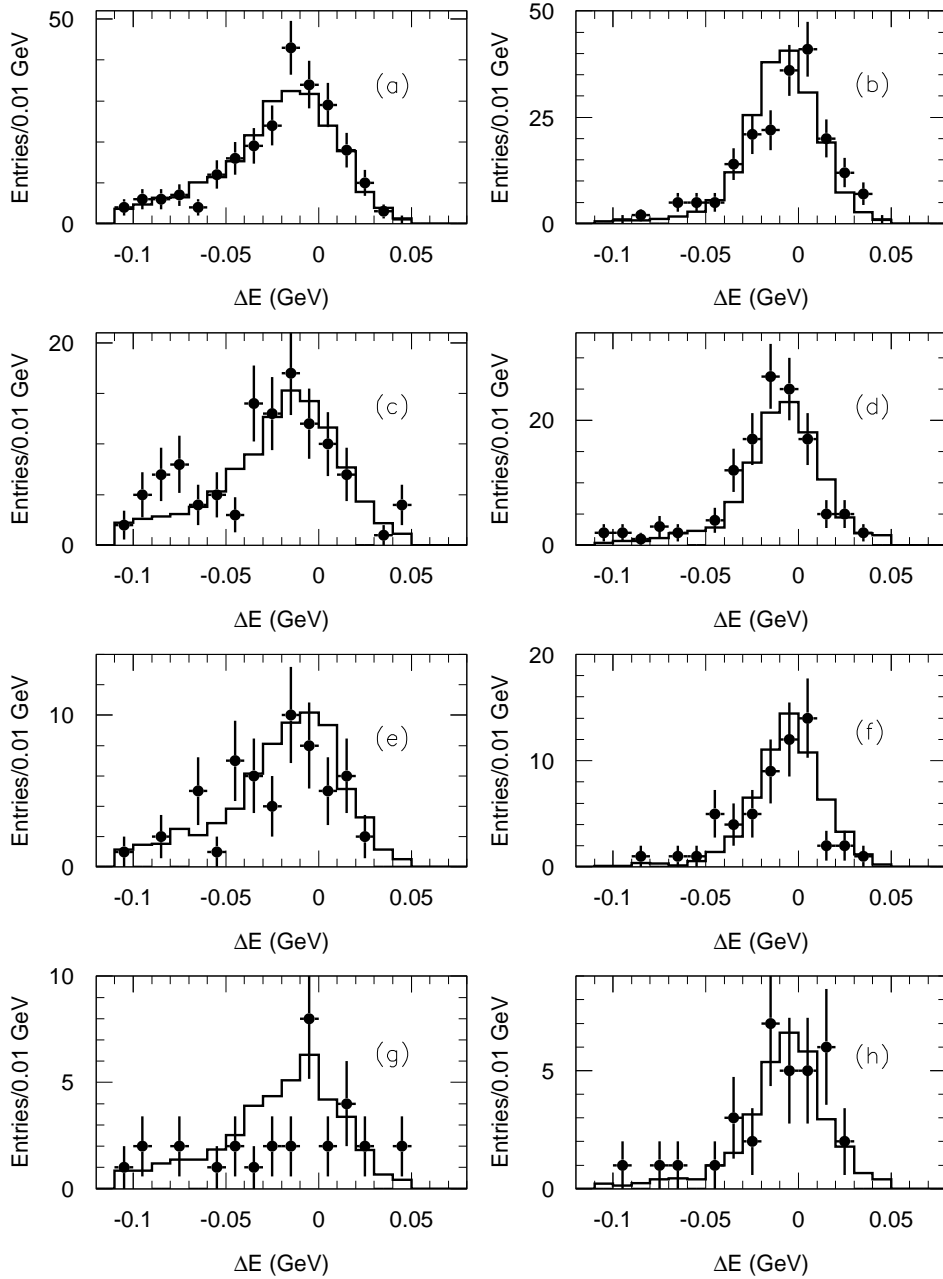


Figure 2: Comparison of ΔE shapes between data and Monte Carlo for the charmonium control samples. (a) $B^+ \rightarrow J/\psi(\rightarrow e^+e^-)K^+$, (b) $B^+ \rightarrow J/\psi(\rightarrow \mu^+\mu^-)K^+$, (c) $B^0 \rightarrow J/\psi(\rightarrow e^+e^-)K^{*0}$, (d) $B^0 \rightarrow J/\psi(\rightarrow \mu^+\mu^-)K^{*0}$, (e) $B^0 \rightarrow J/\psi(\rightarrow e^+e^-)K_S^0$, (f) $B^0 \rightarrow J/\psi(\rightarrow \mu^+\mu^-)K_S^0$, (g) $B^+ \rightarrow J/\psi(\rightarrow e^+e^-)K^{*+}(\rightarrow K_S^0\pi^+)$, and (h) $B^+ \rightarrow J/\psi(\rightarrow \mu^+\mu^-)K^{*+}(\rightarrow K_S^0\pi^+)$. The points with error bars show the on-resonance data, and the solid histograms show the prediction of the charmonium Monte Carlo. All of the analysis selection criteria have been applied except for the charmonium veto, which is reversed. The normalization is absolute.

5 Unbinned Maximum Likelihood Fit

To extract the signal and background yields, we perform an extended unbinned maximum likelihood fit in the ΔE vs. m_{ES} plane. The fit region is defined by $m_{\text{ES}} > 5.2 \text{ GeV}/c^2$ and $|\Delta E| < 0.25 \text{ GeV}$. There are three components in the fit: the signal, the $B\bar{B}$ background, and the continuum $udsc$ background. The likelihood is given by

$$\mathcal{L}(n_{\text{sig}}, n_{B\bar{B}}, n_{\text{cont}}) = \frac{e^{-(n_{\text{sig}} + n_{B\bar{B}} + n_{\text{cont}})}}{N!} \prod_{i=1}^N (n_{\text{sig}} P_i^{\text{sig}} + n_{B\bar{B}} P_i^{B\bar{B}} + n_{\text{cont}} P_i^{\text{cont}}), \quad (1)$$

where N is the total number of events in the fit region; i is an index over the events; and P^{sig} , $P^{B\bar{B}}$, and P^{cont} are the normalized probability density functions (which depend on m_{ES} and ΔE) for the signal, $B\bar{B}$, and continuum background components, respectively. In the fits to the data, the shapes of these three components are fixed (as described below), so that the fit is used only to obtain the yields of these components.

The signal shape, P^{sig} , must describe a number of important properties of the signal events, in particular, the effects of photon radiation from the leptons. The distribution in m_{ES} is essentially a Gaussian centered at the B -meson mass, with a small radiative tail extending to lower values of m_{ES} . The width of this Gaussian, roughly $2.5 \text{ MeV}/c^2$ in both electron and muon channels, is determined primarily by the beam-energy spread. The ΔE distributions are much broader, and the effects of radiation are more pronounced. To describe these shapes and their correlations, we fit Monte Carlo signal events to a product of functions known as ‘‘Crystal Ball shapes’’ [16], one each for m_{ES} and ΔE . Correlations are taken into account by allowing the parameters in the function describing m_{ES} to depend on ΔE . The function describing ΔE is actually somewhat more complicated than the Crystal Ball shape in that a sum of two Gaussians is used, rather than a single Gaussian, to help describe the large radiative effects.

Background events come from two main sources, $\Upsilon(4S) \rightarrow B\bar{B}$ and continuum production of $q\bar{q}$ pairs. The $B\bar{B}$ background shape, $P^{B\bar{B}}$, is parametrized in ΔE as an exponential of a second order polynomial in ΔE multiplied by an Argus function [17] in m_{ES} with the slope parameter taken as a second order polynomial in ΔE . The continuum shape, P^{cont} , is taken as the product of a first order polynomial in ΔE and an Argus function in m_{ES} . The parameters for the $B\bar{B}$ and continuum shapes are determined from fitting our 200 fb^{-1} sample of fast Monte Carlo events. The ability of the fast Monte Carlo to predict these background shapes is checked using the $Ke\mu$ and $K^*e\mu$ control samples in the data (Figure 3). In each final state, the shapes derived from Monte Carlo describe the data well.

Backgrounds that peak under the signal in m_{ES} and ΔE are not included in the fit, because we have suppressed their contributions to a level well under one event.

In the fits we constrain the $B\bar{B}$ and continuum components to be greater than or equal to zero. For the signal yield we have a lower cut-off such that the total fit function is positive to avoid large negative yields in fits where there are no events consistent with signal.

6 Results

Before unblinding the signal region and the near sideband we estimated, based on Monte Carlo and off-resonance data, that there would be a total of 9.1 background events in the signal boxes in the eight modes we analyze. After unblinding, we used the sideband region to determine the

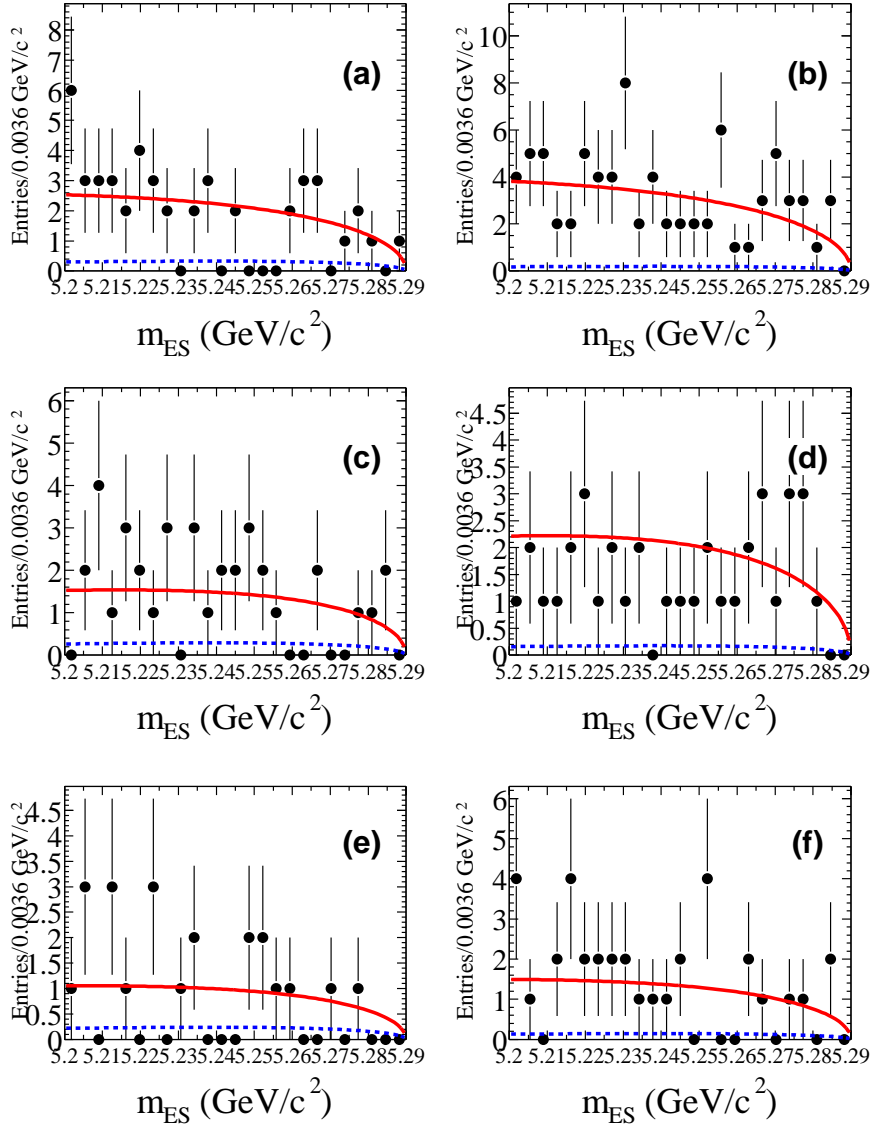


Figure 3: Fitted m_{ES} distributions in the $(K, K^*)e^\pm\mu^\mp$ control sample in data in slices of ΔE : $\Delta E < -0.11$ GeV for (a) $Ke^\pm\mu^\mp$ and (b) $K^{*0}e^\pm\mu^\mp$; $-0.11 < \Delta E < 0.05$ GeV for (c) $Ke^\pm\mu^\mp$ and (d) $K^{*0}e^\pm\mu^\mp$; and $\Delta E > 0.05$ GeV for (e) $Ke^\pm\mu^\mp$ and (f) $K^{*0}e^\pm\mu^\mp$. The dashed lines show the continuum component of the fit, and the solid lines show the sum of continuum and $B\bar{B}$ components.

background in the signal region and found the total background to be 8.4 events. This is in good agreement with our Monte Carlo and off-resonance predictions.

Figure 4 shows the results of unblinding the signal and the near sideband regions. We emphasize that the determination of the signal yields is based on the fit, not on counting the number of events in the signal box. The fit results are shown in Fig. 5 and are summarized in Table 2. By generating multiple toy Monte Carlo samples based on the fit probability density function (see Eq. 1), we determine the signal yield such that 90% of the samples give a number of signal events larger than

Mode	Signal yield	90% C.L. yield	Equiv. bkg.	ϵ (%)	$(\Delta\mathcal{B}/\mathcal{B})_\epsilon$ (%)	$(\Delta\mathcal{B}/\mathcal{B})_{\text{fit}}$ (%)	$\mathcal{B}/10^{-6}$	$\mathcal{B}/10^{-6}$ 90% C.L.
$B^+ \rightarrow K^+ e^+ e^-$	-0.2	3.0	0.6	17.5	± 8.6	± 10.6	-0.1	0.9
$B^+ \rightarrow K^+ \mu^+ \mu^-$	-0.2	2.8	0.4	10.5	± 8.6	± 10.6	-0.1	1.3
$B^0 \rightarrow K^{*0} e^+ e^-$	2.5	6.7	1.8	10.2	± 10.5	± 10.6	1.6	5.0
$B^0 \rightarrow K^{*0} \mu^+ \mu^-$	-0.3	3.6	1.1	8.0	± 10.8	± 10.6	-0.2	3.6
$B^0 \rightarrow K^0 e^+ e^-$	1.3	5.0	0.3	15.7	± 9.3	± 10.6	1.1	4.7
$B^0 \rightarrow K^0 \mu^+ \mu^-$	0.0	2.9	0.1	9.6	± 11.4	± 10.6	0.0	4.5
$B^+ \rightarrow K^{*+} e^+ e^-$	0.1	3.8	0.9	8.5	± 11.4	± 10.6	0.1	10.0
$B^+ \rightarrow K^{*+} \mu^+ \mu^-$	1.0	4.3	0.5	5.8	± 12.0	± 10.6	3.3	17.5
$B^+ \rightarrow K^+ e^\pm \mu^\mp$	-0.6	3.3	1.4	16.8	± 8.6	± 10.6	-0.2	1.0
$B^0 \rightarrow K^{*0} e^\pm \mu^\mp$	0.6	4.5	2.9	11.9	± 10.6	± 10.6	0.3	2.7
$B^0 \rightarrow K^0 e^\pm \mu^\mp$	0.8	3.3	0.7	14.6	± 10.3	± 10.6	0.7	3.3
$B^+ \rightarrow K^{*+} e^\pm \mu^\mp$	-0.4	3.7	0.7	9.3	± 11.7	± 10.6	-0.8	8.7

Table 2: Results from the fits to $B \rightarrow K^{(*)}\ell^+\ell^-$ modes. The yield refers to the number of signal events given by the fit. The next column gives the 90% C.L. upper limit signal yield. The contribution of the background to the error on the signal yield, expressed as an equivalent background yield (see text), is reported in the next column. ϵ is the signal efficiency, defined as the efficiency for the signal events to be in the fit region and does not include the branching fractions of secondary decays. The systematic error on the efficiency, $(\Delta\mathcal{B}/\mathcal{B})_\epsilon$, and on the signal yield from the fit, $(\Delta\mathcal{B}/\mathcal{B})_{\text{fit}}$, are listed. The last two columns give the central values of the branching fractions (\mathcal{B}) and the preliminary upper limits on the individual modes at 90% C.L.

that observed in the data. For the modes where we observed a negative yield, we place the 90% confidence level limit assuming zero events were observed. Table 2 lists an equivalent background yield determined as the square of the error on the signal yield in toy Monte Carlo simulations in which only the background components were included. Table 2 also includes the results for the lepton-number-violating decays $B \rightarrow K^{(*)}e\mu$, where the signal efficiencies were determined from a phase space Monte Carlo simulation of these decays.

There are two main categories of systematic uncertainties that affect the limits: uncertainties from the fit on the extracted number of signal events and uncertainties on the signal efficiency. Sources of systematic uncertainties are summarized in Table 3.

The sources of systematic uncertainty affecting the extraction of the signal yield are the errors associated with the choice of the background and signal parametrization in the fit. To evaluate the systematic uncertainty on the background shape, we took the difference between the nominal result for the 90% C.L. event yield and the largest deviation found if one allows the background shape to be given either by a pure $B\bar{B}$ or a pure continuum shape. We assign an error of $\pm 7\%$ to the uncertainty in the knowledge of the background shape. The systematic error on the signal parametrization is established by varying the signal shape using the parameters obtained from fitting the charmonium control sample, and is of the order $\pm 8\%$.

In setting the upper limit, the systematic errors on the efficiency, $(\Delta\mathcal{B}/\mathcal{B})_\epsilon$, and on the signal yield from the fit, $(\Delta\mathcal{B}/\mathcal{B})_{\text{fit}}$, are added in quadrature, and the limit is increased by the corresponding factor.

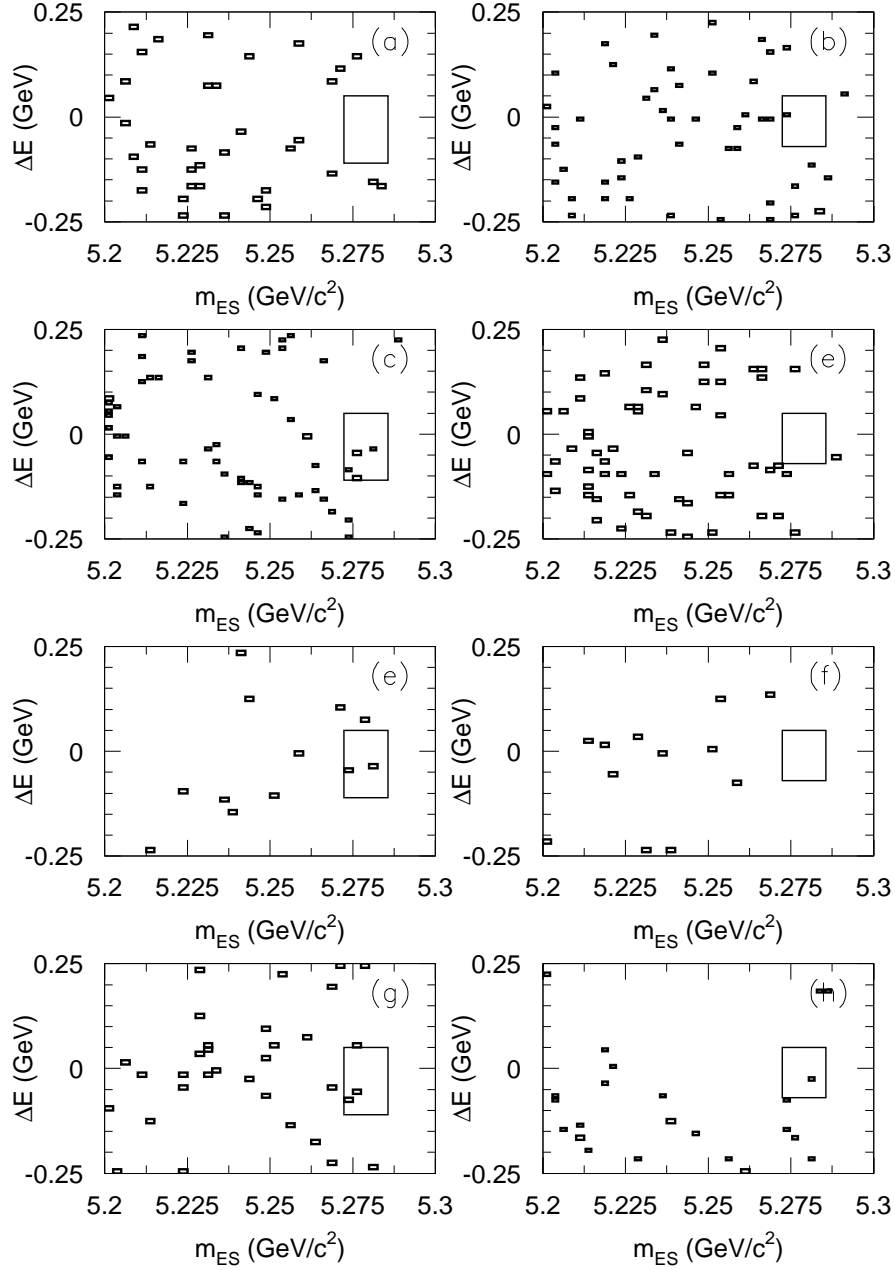


Figure 4: Scatterplots of ΔE vs. m_{ES} after all analysis cuts in (a) $B^+ \rightarrow K^+ e^+ e^-$, (b) $B^+ \rightarrow K^+ \mu^+ \mu^-$, (c) $B^0 \rightarrow K^{*0} e^+ e^-$, (d) $B^0 \rightarrow K^{*0} \mu^+ \mu^-$, (e) $B^0 \rightarrow K_S^0 e^+ e^-$, (f) $B^0 \rightarrow K_S^0 \mu^+ \mu^-$, (g) $B^+ \rightarrow K^{*+} (\rightarrow K_S^0 \pi^+) e^+ e^-$, and (h) $B^+ \rightarrow K^{*+} (\rightarrow K_S^0 \pi^+) \mu^+ \mu^-$. The small rectangle indicates the signal region, which is used only for optimizing event selection criteria.

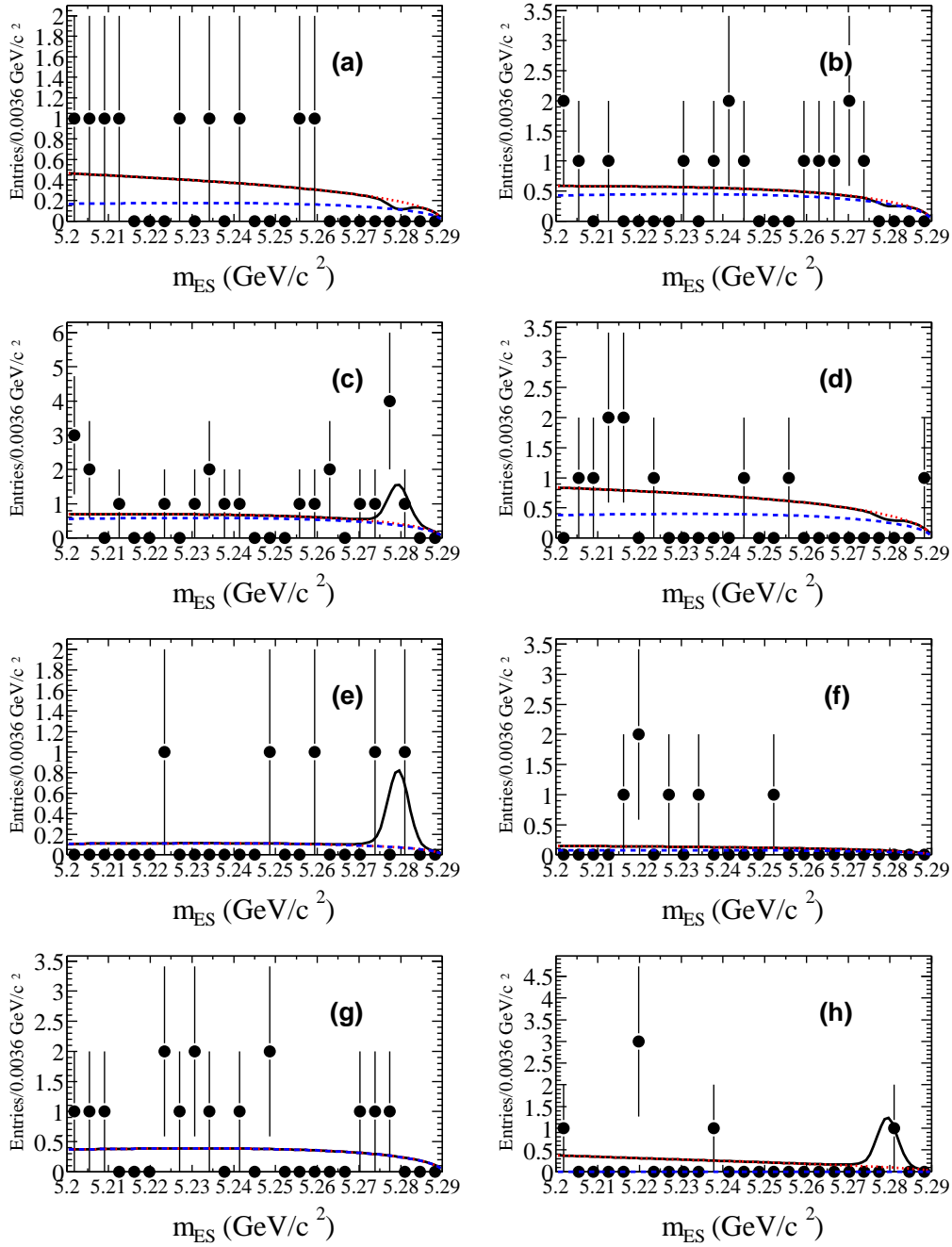


Figure 5: Fitted m_{ES} distributions in the ΔE signal region for (a) $B^+ \rightarrow K^+ e^+ e^-$, (b) $B^+ \rightarrow K^+ \mu^+ \mu^-$, (c) $B^0 \rightarrow K^{*0} e^+ e^-$, (d) $B^0 \rightarrow K^{*0} \mu^+ \mu^-$, (e) $B^0 \rightarrow K_S^0 e^+ e^-$, (f) $B^0 \rightarrow K_S^0 \mu^+ \mu^-$, (g) $B^+ \rightarrow K^{*+} (\rightarrow K_S^0 \pi^+) e^+ e^-$, and (h) $B^+ \rightarrow K^{*+} (\rightarrow K_S^0 \pi^+) \mu^+ \mu^-$. The dashed lines show the continuum component of the fits, the dotted lines show the sum of continuum and $B\bar{B}$ components, and the solid lines show the sum of background and signal components of the fit.

Source of systematic uncertainty	$\Delta\mathcal{B}/\mathcal{B}$ (%)
Lepton tracking efficiency	± 1.2
Pion from K^* tracking efficiency	± 2.0
Tracking efficiency for other tracks	± 1.3
Electron identification	± 2.7
Muon identification	± 2.0
Kaon and pion identification	± 2.0
Monte Carlo statistics for signal	$\pm(3.0 \text{ to } 5.0)$
Continuum suppression cut	± 2.0
$B\bar{B}$ suppression cut	± 3.0
K_S selection	± 4.0
Modeling of signal kinematic distributions	± 5.0
Number of $B\bar{B}$ pairs	± 1.6
Background shapes	± 7.0
Signal shapes	± 8.0

Table 3: Sources of systematic uncertainties on the limits.

7 Combined Results and Conclusions

We average the electron and muon channels to determine the average branching fractions $\mathcal{B}(B \rightarrow K\ell^+\ell^-)$ and $\mathcal{B}(B \rightarrow K^*\ell^+\ell^-)$. The modes are combined using the likelihood fit where a combined likelihood is formed as a product of the likelihoods of the individual modes. The fit extracts a combined signal event yield. For the averaging of modes with K^* mesons the ratio of branching fractions $\mathcal{B}(B \rightarrow K^*e^+e^-)/\mathcal{B}(B \rightarrow K^*\mu^+\mu^-)$ from the model of Ali *et al.* (see Table 1) is used to weight the yield in the muon mode relative to the electron mode. The extracted yield corresponds to the electron mode. The combined fits give

$$\begin{aligned}\mathcal{B}(B \rightarrow K\ell^+\ell^-) &= (0.0 \pm 0.3(\text{stat.})) \times 10^{-6} \\ \mathcal{B}(B \rightarrow K^*\ell^+\ell^-) &= (0.7 \pm 1.1(\text{stat.})) \times 10^{-6}.\end{aligned}$$

As there is no evidence for a signal we evaluate the upper limits on these combined modes and obtain the preliminary results

$$\begin{aligned}\mathcal{B}(B \rightarrow K\ell^+\ell^-) &< 0.6 \times 10^{-6} \text{ at } 90\% \text{ C.L.} \\ \mathcal{B}(B \rightarrow K^*\ell^+\ell^-) &< 2.5 \times 10^{-6} \text{ at } 90\% \text{ C.L.}\end{aligned}$$

based on the analysis of a sample of $22.7 \times 10^6 \Upsilon(4S) \rightarrow B\bar{B}$ decays in the *BABAR* 1999-2000 data set. These limits represent a significant improvement over previous results [18, 19, 20] and are at the same level as the Standard Model predictions listed in Table 1.

8 Acknowledgements

We are grateful for the extraordinary contributions of our PEP-II colleagues in achieving the excellent luminosity and machine conditions that have made this work possible. The collaborating institutions wish to thank SLAC for its support and the kind hospitality extended to them. This

work is supported by the US Department of Energy and National Science Foundation, the Natural Sciences and Engineering Research Council (Canada), Institute of High Energy Physics (China), the Commissariat à l’Energie Atomique and Institut National de Physique Nucléaire et de Physique des Particules (France), the Bundesministerium für Bildung und Forschung (Germany), the Istituto Nazionale di Fisica Nucleare (Italy), the Research Council of Norway, the Ministry of Science and Technology of the Russian Federation, and the Particle Physics and Astronomy Research Council (United Kingdom). Individuals have received support from the Swiss National Science Foundation, the A. P. Sloan Foundation, the Research Corporation, and the Alexander von Humboldt Foundation.

References

- [1] CLEO Collaboration (R. Ammar *et al.*), Phys. Rev. Lett. **71**, 674 (1993).
- [2] CLEO Collaboration (M.S. Alam *et al.*), Phys. Rev. Lett. **74**, 2885 (1995).
- [3] A. Ali, P. Ball, L.T. Handoko, and G. Hiller, Phys. Rev. D **61**, 074024 (2000); hep-ph/9910221.
- [4] T.M. Aliev, A. Ozpineci and M. Savci, Phys. Rev. D **56**, 4260 (1997); hep-ph/9612480.
- [5] T.M. Aliev, C.S. Kim, and Y.G. Kim, Phys. Rev. D **62**, 014026 (2000); hep-ph/9910501.
- [6] D. Melikhov, N. Nikitin, and S. Simula, Phys. Lett. B **410**, 290 (1997); hep-ph/9704628. We have scaled these results up by the ratio $(0.04/0.033)^2$.
- [7] D. Melikhov and B. Stech, Phys. Rev. D **62**, 014006 (2000); hep-ph/0001113.
- [8] P. Colangelo, F. De Fazio, P. Santorelli, and E. Scrimieri, Phys. Rev. D **53**, 3672 (1996); Erratum–*ibid.* D**57**, 3186 (1998); hep-ph/951043.
- [9] P. Colangelo *et al.*, Eur. Phys. J. C **8**, 81 (1999); hep-ph/9809372.
- [10] G. Buchalla, A. Buras, and M. Lautenbacher, Rev. Mod. Phys. **68**, 1125 (1996).
- [11] BABAR Collaboration (B. Aubert *et al.*), SLAC-PUB-8569, submitted to Nucl. Instrum. Methods (2001); hep-ex/0105044.
- [12] “GEANT–Detector Description and Simulation Tool”, CERN Program Library Long Writeup W5013, (1995).
- [13] D.J. Lange, Nucl. Instrum. Methods A **462**, 152 (2001).
- [14] E. Barberio and Z. Was, Comput. Phys. Commun. **79**, 291 (1994).
- [15] G.C. Fox and S. Wolfram, Phys. Rev. Lett. **41**, 1581 (1978).
- [16] T. Skwarnicki, *A Study of the Radiative Cascade Transitions Between the Upsilon-Prime and Upsilon Resonances*, DESY F31-86-02 (thesis, unpublished) (1986).
- [17] ARGUS Collaboration (H. Albrecht *et al.*), Phys. Lett. B **185**, 218 (1987).
- [18] CDF Collaboration (T. Affolder *et al.*), Phys. Rev. Lett. **83**, 3378 (1999).

- [19] CLEO Collaboration (S. Anderson *et al.*), submitted to Phys. Rev. Lett.; hep-ex/0106060.
- [20] T. Iijima for the Belle Collaboration, to appear in the Proceedings of the 4th International Conference on B Physics and CP Violation, Ago Town, Mie Prefecture, Japan, February 19-23 (2001); hep-ex/0105005.